Computational Condensed Matter 33 (2022) e00737

Contents lists available at ScienceDirect

Computational Condensed Matter

journal homepage: www.elsevier.com/locate/cocom

Ab-initio calculations of the structural, electronic and optical response of $KXCl_3$ (X = be, Ca and Sr) for optoelectronic applications

Ayesha Zia [a], G. Murtaza [a,**], Khawar Ismail [a], R.M. Arif Khalil [b,***], Muhammad Iqbal Hussain [c,*]

[a] Centre for Advanced Studies in Physics GC University Lahore, 54000, Pakistan
[b] Materials Simulation Research Laboratory (MSRL), Department of Physics, Bahauddin Zakariya University Multan, 60800, Pakistan
[c] Department of Physics, University of Education, Lahore, 54000, Pakistan

ARTICLE INFO

Keywords:
Optoelectronics
DFT
Spintronics

ABSTRACT

Ab-initio studies of crystal structure, optoelectronic and mechanical response of potassium-based perovskite $KXCl_3$ (X = Be, Ca and Sr) compounds have been employed using the quantum based Density Functional Theory (DFT) within the framework of WIEN2K code. The Generalized Gradient Approximation within the scheme of Perdew-Burke- Ernzerhof (PBE-GGA) exchange-correlation approximation is used to calculate the exchange-correlation potential of these compounds. The band structures and Density of States (DOS) are computed by using these approximations. The Band structure and density of state DOS of studied compounds show the wide bandgap semiconductor behavior and these semiconductor materials have indirect band gap semiconductor materials nature. The optical response of the compounds can be checked in terms of the real and the imaginary parts of the dielectric function; and refractive index, extinction coefficient thermal conductivity reflectivity and energy loss function. This frequency dependent optical parameter of studied compounds in the ultraviolet energies region makes them valuable material for optoelectronic devices. Therefore, this potassium based perovskite $KXCl_3$ (X = Be, Ca and Sr) compounds may be used for the fabrication of a transparent material and optoelectronic devices. . According to Born's criterion, $KCaCl_3$ is found to be brittle while $KBeCl_3$ and $KSrCl_3$ are established as ductile material for different mechanical applications. Finally, theoretically calculated results agree well theoretically and experimental available literature review.

1. Introduction

Gustav Rose discovered the perovskite structure in the Ural Mountains in 1839 and named it after Russian mineralogist Pervoski (1792–1856) [1]. Mineralogist Perovski reported calcium titanate ($CaTiO_3$), which was widely understood to be the source of perovskite. Materials with the same crystal structure as $CaTiO_3$ were called "perovskite materials" (structure). Halides having the perovskite structure, both organic and inorganic, have caught the interest of the photovoltaic community since late 2012. The importance of evaluating and analyzing the potential of this fascinating technology, which has energized the photovoltaic research community, cannot be underestimated. Even though this class of materials has been extensively investigated for decades, organic/inorganic metal halides are effective light absorbers [2–4]. The typical stoichiometry of the perovskite structure is ABX_3, where A and B are the metallic cations, and X can be either oxygen or halide elements (F, Cl, Br, and I) [5]. The halide based-perovskites semiconductor materials are an important class of the perovskite family. The perovskite type semiconductor materials are considered the potential candidate for optoelectronic and solar cell applications [6], because of their low cost value and better efficiency of optical response that are directly related to the band gap properties of the materials [7–9]

These materials have attracted attention for optoelectronic and photovoltaic applications because of their unusual physical properties including their high absorption coefficient, long-range ambipolar charge transfer, low exciton-binding energy, high dielectric constant, and ferroelectric capabilities [10,11]. Multiple classes of perovskite materials were examined in-depth; however, halide perovskites (ABX_3) are the most promising materials yet to study widely. Organic–inorganic

* Corresponding author.
** Corresponding author.
*** Corresponding author.
E-mail addresses: gmrai@gcu.edu.pk (G. Murtaza), muhammadarif@bzu.edu.pk (R.M.A. Khalil), miqbal@ue.edu.pk (M.I. Hussain).

https://doi.org/10.1016/j.cocom.2022.e00737
Received 22 April 2022; Received in revised form 16 August 2022; Accepted 19 August 2022
Available online 2 September 2022

lead halides were also investigated for thin-film LEDs and field effect transistor (FET) applications due to the strong excitonic characteristics of perovskite materials (layered) [12,13].

In 2019 Mahmood et al. [14] investigated Cesium based bromides mechanical, optical, thermoelectric and thermodynamic characteristics systematically using the most comprehensive DFT based WIEN2K code for elucidating the energy renewable device applications. Very recently in 2021 Lamichhane et al. [15] have examined halide perovskites, which have the potential to be used in solar cells and reported the effect of cation and anion substitution on their overall properties of halide perovskites. They studied the structural, mechanical, and electro-optical characteristics of ABX_3 (A = K, Rb, Cs; B = Ge, Sn, Pb; and X = Cl, Br, I) under isosymmetric compression in his study. All the calculations are performed with generalized gradient approximation schemes. All computations are made using extended gradient approximation methods. The use of isosymmetric stress resists the external circumstances, allowing these powerful solar materials to act reliably. LEDs, solar cells, and other optoelectronic devices may benefit from this knowledge. In 2019 *Pitriana* et al. [16] used first-principle calculations and examine the band structure and crystal binding properties of the all-inorganic perovskite $APbBr_3$. Their findings show that, with the exception of $LiPbBr_3$ and $NaPbBr_3$ perovskites, the A^+ cations play no major role in the interband photoexcitation, photovoltaic, or charge transport processes. 1n 2019 Sabir et al. [17] studied properties of $CsMO_3$ (M = Nb, Ta) compounds explored by using FP-LAPW method implemented in the DFT based WIEN2K code. This work explains the electronic, optical, mechanical, thermodynamic, and thermoelectric properties and exhibit that the increasing values of electrical conductivity and power factor with temperature are best suited for thermoelectric and optoelectronic applications [18]. investigated the structural, electronic and optical properties to identify the suitability of inorganic lead-free halide perovskites $ASnX_3$ (A = Rb, K; X = Cl, Br) as solar materials.

The goal of this comparison study is to investigate structural, optoelectronic and mechanical response of potassium-based perovskites $KXCl_3$ (X = Be, Ca, Sr) compounds by employing the quantum-based Density Functional Theory (DFT) within WIEN2K code.

2. Computational details

The structural, electronic, and optical properties of $KXCl_3$ (X = Be, Ca, and Sr) are investigated using Local Orbital and Full Potential Linearized Augmented Plane-Wave (LO + FP-LAPW) method [19]. The exchange-correlation potential and optimal ground state parameters were studied using the PBE-GGA approximation [20]. We solved the birch Murnaghan equation of state to optimize cubic structures $KXCl_3$ (X = Be, Ca, and Sr). The bandgap and electronic characteristics are tuned using Tran-Blaha-modified Becke-Johnson (TB-mBJ) exchange potential [21]. The basis set in (RMT) is the radial solution of the single-particle Schrödinger equation and energy derivatives multiplied by the smallest atom in the unit volume of the crystal structure. The energy convergence of crystal structure is defined by $R_{MT} \times K_{max} = 8$, here the R_{MT} and K_{max} show the radius of the muffin tin sphere and the magnitude of the largest plane wave vector of the atoms in crystal structure, respectively. The highest value of spherical harmonics at atomic sites is $L_{max} = 10$, and the charge density Fourier expansion value $G_{max} = 12$ (a.u)$^{-1}$. The RMT values for Be, Ca, and Sr are (1.5, 2.0, and 2.1 a.u.) while for both K and Cl atoms it is 1.9. The Brillouin area of the considered compounds is chosen to contain 100 K points, and the self-consisting field (SCF) cycle is performed until the unit crystal structure's total energy converging value is less than 10^{-5} Ry [22]. Optical properties were calculated by solving Kramers–Kronig the well familiar relations [23]. So far as mechanical stability, the elastic constants are calculated while using the Born stability criteria [24].

3. Results and discussions

3.1. Structural properties

The crystal structures of $KXCl_3$ (X = Be, Ca, and Sr) compounds are shown in Fig. 1. The information about structure stability, lattice constants and the atomic arrangement of the constituent elements is very important for the fabrication of device applications. The unit cell structure of these compounds such as $KXCl_3$ (X = Be, Ca, and Sr) are stable in the cubic phase with space group 221 (Pm-3m). As shown in Fig. 2, the graphs of energy versus volume ensure stability of these compounds. The ground state minimum energy of $KXCl_3$ (X = Be, Ca, and Sr) is computed as a function of unit cell volume by using the following Birch–Murnagahan's state equation [25].

$$E(V) - E(V_o) = \left(\frac{B_o V}{B_o'}\right)\left[\frac{\left(\frac{V_o}{V}\right)^{B_o'}}{B_o} + 1\right] - \left[\frac{B_o V}{B_o'}\right] \quad (1)$$

where, $E(V)$ is the value of ground state energy with volume V of a unit cell. $E(V_o)$ Indicate the ground state energy with V_o at zero pressure. B_o symbolizes bulk modulus. B_o' represents the derivative of bulk modulus at zero pressure. The computed values of equilibrium lattice parameters, bulk modulus, and its pressure derivative for these compounds are given in Table 1. Theoretical data for our materials is well supported by computational calculations made for $XCaF_3$ (X = K, Rb, Cs) in cubic phase and $KCaF_3$ [25,26] as well as experimentally available literature about $KCaF_3$, $RbCaF_3$, and computational and experimental work on $KCaX_3$ (X = F and Cl) compounds [8,27]. The use of distinct exchange-correlation potential may account for the modest discrepancies in computations between this work and previous studies.

3.2. Electronic properties

3.2.1. Band structure

The electronic band structure of any material gives information about energy band gap (E_g) value along with the direct and indirect band gap nature of compounds. Additionally, the band structure implies important information about the materials, whether they are semiconductors, metals, or insulators. The electronic band structures of the potassium-based perovskite $KXCl_3$ (X = Be, Ca, and Sr) are depicted in Fig. 3 which shows high symmetry directions in the first Brillouin zone (BZ).

The electronic band structure of $KXCl_3$ (X = Be, Ca and Sr) is determined along the symmetry directions (R Γ X M and Γ) in an irreducible BZ by using PBE-GGA. It has been observed that maxima of the valence band lies at M symmetry point of the first BZ where minima of the conduction band is found at Γ symmetry point near the Fermi level (E_F) in first BZ. So, these compounds are indirect band gap semiconductors. The double-headed brown line in Fig. 3, ensures the indirect band gap between the conduction band and valence band. For $KBeCl_3$, $KCaCl_3$, and KSrCl3, the estimated values of indirect E_g are 1.907, 3.849 and 4.346 eV, respectively. Although the calculated value of E_g for $KCaF_3$ = 5.95 eV [29] and in experimental studies [30] it was reported as 6.13 eV. The formerly reported values show that our results about E_g are in good agreement with the theoretically explored [28] and experimental value of E_g Ref. [27]. The values of E_g for $KXCl_3$ (X = Be, Ca, and Sr) at various symmetric points in the first BZ are presented under Table 2.

3.2.2. Density of states

To visualize and explain the basis of electronic band structures and to understand deeply the electronic properties of studied compounds, we have investigated the total density of states (TDOS) and partial density of states (PDOS). The density of states define the number of available

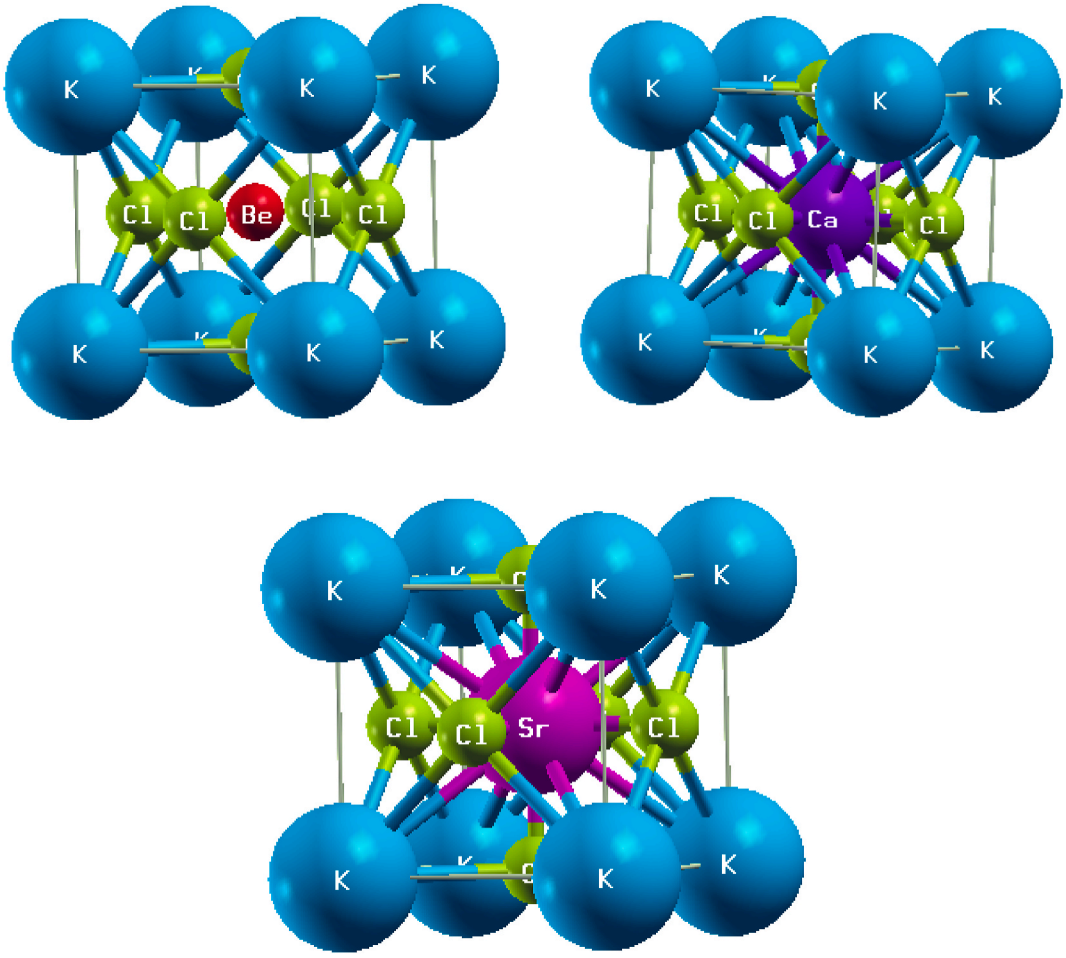

Fig. 1. The cubic unit cell structures of $KXCl_3$ (X = Be, Ca and Sr) compounds.

states per unit volume in an energy level in which an electron can occupy. Fig. 4 displays the total and partial density of states for $KXCl_3$ (Be, Ca, and Sr). In maxima of the valence band of $KBeCl_3$, *p*-state of Cl shows major contribution at −0.03 eV and *p*-state of Be shows minor contribution at −0.09 eV. *s*-states of K and Be show their contribution at −0.07 eV and −0.10 eV, respectively. On other hand, minima of conduction band constitute *p*-state of Cl with its major contribution at 0.03 eV and shows minor contribution at 0.04 eV. *s*-orbitals of K, Be and Cl didn't show any contribution. In $KCaCl_3$, maxima of the valence band *p*-states of Cl and Ca show the same contribution at the energy of −0.21 eV. *s*-states of K and Ca show their minor contribution at −0.19 eV and −0.24 eV, respectively. Moreover, minima of conduction band *p*-state of Cl and Ca show contribution at 0.26 eV and 0.27 eV. While *s*-orbitals of K and Ca show contribution at 0.28 eV and 0.26 eV. So far as maxima of the valence band of $KSrCl_3$, *s*-state of K has shown weak contribution at −0.19 eV energy and *d*-state of Sr shows major contribution at −0.21 eV here Cl seems insignificant in the valence band formation. However, *s*-states of K and Cl are found to be contributing at 0.28 eV and 0.15 eV. *d*-states of Sr and *p*-states of Cl have shown their weak contribution at 0.26 eV and 0.15 eV, respectively.

3.3. Optical properties

The frequency-dependent optical properties of potassium-based perovskites $KXCl_3$ (X = Be, Ca and Sr) can be demonstrated by the dielectric function $\epsilon(\omega) = \epsilon_1(\omega) + i\epsilon_2(\omega)$; where $\epsilon_1(\omega)$ and $\epsilon_2(\omega)$ represent the real and imaginary parts of the dielectric function, absorption coefficient $a(\omega)$, extinction coefficient $k(\omega)$, reflectivity $R(\omega)$, refraction index $n(\omega)$ and energy loss function $L(\omega)$. These frequency dependent parameters play a significant role to check the efficiency of nano-electronics and optoelectronic devices [31].

The imaginary part $\epsilon_2(\omega)$ of dielectric function is closely connected to the electrical band structure; which provides information about the absorption of light [32]. It is frequently calculated by the accumulation of all potential transitions from occupied to unoccupied states while taking the relevant transition matrix element into account as explained by Ambrosch-Draxl and co-workers in their earlier reports [33,34]. The computed $\epsilon_2(\omega)$ for $KXCl_3$ (Be, Ca, and Sr) is shown in Fig. 5. We may confidently argue three threshold spots in the spectrum at 2.5 eV, 3.5 eV and 3.0 eV for $KBeCl_3$, $KCaCl_3$, and $KSrCl_3$, respectively, to the electronic transition between the valence and the conduction bands. These transitions occur from X-*p* (Be, Ca and Sr) states to Cl-*p* with contributions from K-*s* states in the conduction band. The major peak in the spectrum is found to be situated at 9.07 eV, 11.44 eV and 9.72 eV for $KBeCl_3$, $KCaCl_3$ and $KSrCl_3$, respectively. It is clear from Fig. 5 that $KSrCl_3$ have higher absorption than $KBeCl_3$ and $KCaCl_3$. Which ensures that comparatively in case of $KSrCl_3$ the dissipation of incident light is more in the form of excitation between valence to the conduction band.

The real part $\epsilon_1(\omega)$ of the dielectric function contains information about a material's polarization. Which can be calculated with the help of an imaginary part $\varepsilon_2(\omega)$ by Kramers–Kronig model [23]. Fig. 6 shows the frequency-dependent dielectric function with its $\epsilon_1(\omega)$. Static dielectric constant $\epsilon_1(0)$ is determined to be 2.96, 1.91, and 3.67 for $KBeCl_3$, $KCaCl_3$, and $KSrCl_3$, respectively. At higher energies, $\epsilon_1(\omega)$ increases to 3.60 at 4.12 eV for $KBeCl_3$, 2.60 at 6.62 eV for $KCaCl_3$ and 8.5 at 6.50 eV for $KSrCl_3$. In this work, the results agree well with the available

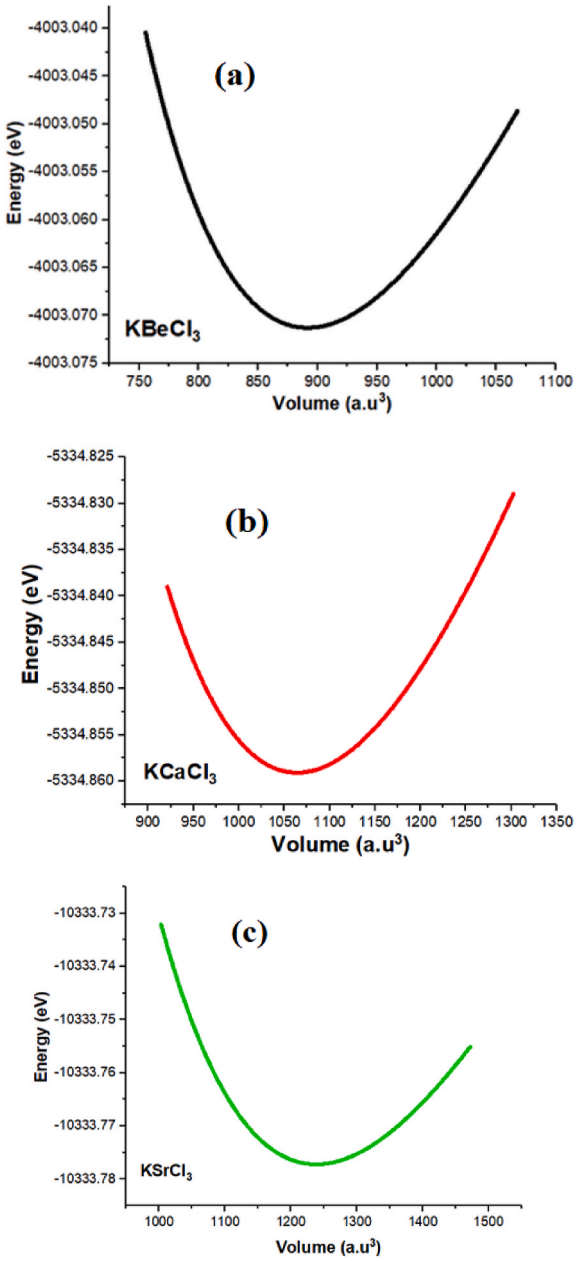

Fig. 2. Optimized graph of energy as a function of volume for (a) $KBeCl_3$ (b) $KCaCl_3$ and (c) $KSrCl_3$.

Table 1
Lattice constant a (Å), bulk modulus B_o (GPa) and bulk modulus derivative $B_0^{'}$ of $KBeCl_3$, $KCaCl_3$ and $KSrCl_3$ compounds.

Compounds	a (Å)	B_0 (GPa)	$B_0^{'}$
$KBeCl_3$	4.6175	46.5333	4.333
$KCaCl_3$	5.3093	46.5333	4.3721
$KSrCl_3$	5.6631	20.9014	4.3697
Other calculations	5.410[c]	46.98[c]	4.5475[c]
	4.4584[b]		
	4.47[a]		
	4.32[d]		

[a] Ref. [25].
[b] Ref. [26].
[c] Ref. [8,27].
[d] Ref. [28].

experimental literature results for $KCaCl_3$ [30]. The indirect band gaps of $KBeCl_3$, $KCaCl_3$, and $KSrCl_3$ are 1.907 eV, 3.849 eV, and 4.346 eV, respectively. Other compounds with similar band gaps and low values of $\epsilon_1(0)$, as we examined for our studied compounds, have been used in optoelectronic applications. Thus, our computed results are in line with previous findings in the literature [35,36] which support the possibility of using our investigated materials for optoelectronic applications.

The refractive index $n(\omega)$ is the ratio of a given material's speed of light to the speed of light in a vacuum that refers to the capacity of the matter to allow electromagnetic radiations to pass through it. Higher value of the refractive index indicates that materials are opaque and vice versa [36]. Fig. 7 shows $n(\omega)$ of $KXCl_3$, where 1.72, 0.1 and 1.9 are discovered to be the zero-frequency refractive indices for $KXCl_3$ (Be, Ca, Sr). As a result, the highest values of $n(\omega)$ were found to be 1.8, 0.33, and 3.0 for $KXCl_3$ (Be, Ca, Sr), respectively. The results show that $KSrCl_3$ and $KBeCl_3$ are comparatively more opaque materials.

Behavior of the extinction coefficient $k(\omega)$ is similar to that of the $\varepsilon_2(\omega)$, which tells us how much a material will absorb light radiations. So, both are co-related by this relation $2nk = \varepsilon_2(\omega)$ [36]. Our results pertaining to the $k(\omega)$ are presented in Fig. 8. The local maxima of $k(\omega)$ were found to be 1.5 at 9.9 eV and 12 eV for $KBeCl_3$, 1.37 at 11.19 eV for $KCaCl_3$ and 2.0 at 11.41 for $KSrCl_3$.

The reflectivity of any material can demonstrate reflection of incident light from surface of the material [31]. The spectrum of reflectivity R(ω) is shown in Fig. 9. The static value of the reflectively R(0) for $KBeCl_3$, $KCaCl_3$, and $KSrCl_3$ are 4%, 3%, and 9.8%, respectively. The relatively low reflectivity of these materials suggests that they are opaque in IR, visible, and low frequency end of the UV spectrum. Maximum reflectivity values for $KBeCl_3$ are 27% at 9.1 eV, 15% at 6.6 eV for $KCaCl_3$ and 33% at 10 eV for KSsrCl$_3$.

The energy loss function L(ω) is a significant feature explaining the energy loss of a speedy electron passing through a matter either by dispersion scattering or heating [28]. The varieties of energy loss deliver valued shreds of evidence around Plasmon excitation, intra-band and interband transitions. The maximum peaks indicate the plasmon excitations related to plasmon frequency. Rapid electrons passing through surface of $KXCl_3$ (Be, Ca, and Sr) may lose energy according to the energy curve depicted in Fig. 10. The response of this function is frequently high at the plasmon frequency. $KBeCl_3$, $KCaCl_3$ and $KSrCl_3$ have shown energy loss peaks at 11.22 eV, 11.46 eV and 10.84 eV, respectively. According to our computed energy loss function, these sharp peaks correlate to a sudden drop in the reflectivity spectrum (Fig. 9).

The absorption coefficient $\alpha(\omega)$ relates the capacity of a material to absorb the incident photon of definite energy. The absorption constant can be computed by the imaginary part of the dielectric function. The absorption peaks occur due to the interaction between photons and electrons and also occur due to intraband and interband transitions. The absorption is co-related to the extinction coefficient by the relation $\alpha(\omega) = \frac{4\pi k(\omega)}{\lambda}$. The $\alpha(\omega)$ for three studied compounds is shown in Fig. 11. At high energies, there is a very strong absorption peak, which is quite intriguing to see. Comparatively $KSrCl_3$ has shown large scale absorption than other two compounds. They have shown high absorption at various spells of energy in the energy range from visible to ultra-violet. Maximum values of absorption coefficient and refractive index, fewer values of reflectivity, and energy loss function make them potential materials for optoelectronic applications.

3.4. Elastic properties

Elastic constants C_{ij} are crucial factors because they indicate how the material responds when pressure is applied to it [24]. Elastic properties of the compounds are important to study in order to make them useful materials for optoelectronic applications. However, for mechanical stability, the elastic constants must follow the Born stability criteria [24]. For cubic materials, three independent constants C_{11}, C_{44} and C_{22}

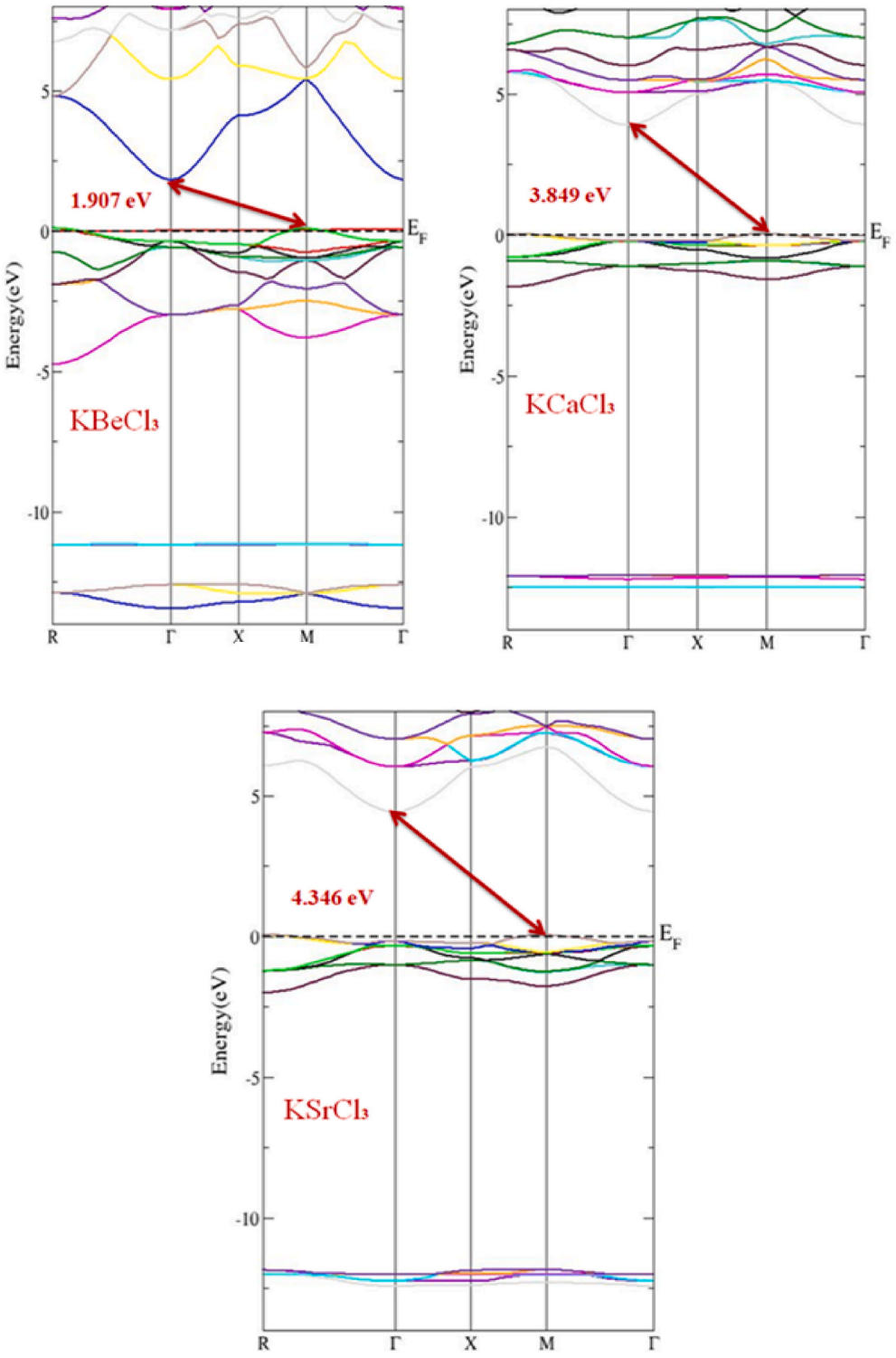

Fig. 3. The indirect band gap of potassium based perovskites i.e. $KBeCl_3$, $KCaCl_3$ and $KSrCl_3$ by using TB-mBJ functional.

Table 2
Band-gap energies of $KBeCl_3$, $KCaCl_3$ and $KSrCl_3$ compounds at high symmetry points.

Compounds	E^{R-R}	$E^{\Gamma-\Gamma}$	E^{X-X}	E^{M-M}	$E^{R-\Gamma}$	$E^{X-\Gamma}$	$E^{M-\Gamma}$
$KBeCl_3$	4.665	2.160	4.541	5.416	1.902	2.882	1.907
$KCaCl_3$	5.719	4.099	5.155	5.372	3.845	4.099	3.849
$KSrCl_3$	6.015	4.591	6.259	6.648	4.199	4.615	4.346

are required to fulfill the following stability criteria for cubic crystal [37]:

$$C_{11} > 0,\ C_{44} > 0,\ C_{11} > |C_{12}|,\ (C_{11}+2C_{12}) > 0 \quad (2)$$

Moreover, elastic constants calculations proved that cubic compounds $KBeCl_3$, $KCaCl_3$ and $KSrCl_3$ are mechanically stable because they satisfy the stability criteria. Values of elastic constants are represented in Table 3. Elastic constant data is also used to measure the shear and bulk moduli through Reuss [38] and Voigt approximation [39] method. The

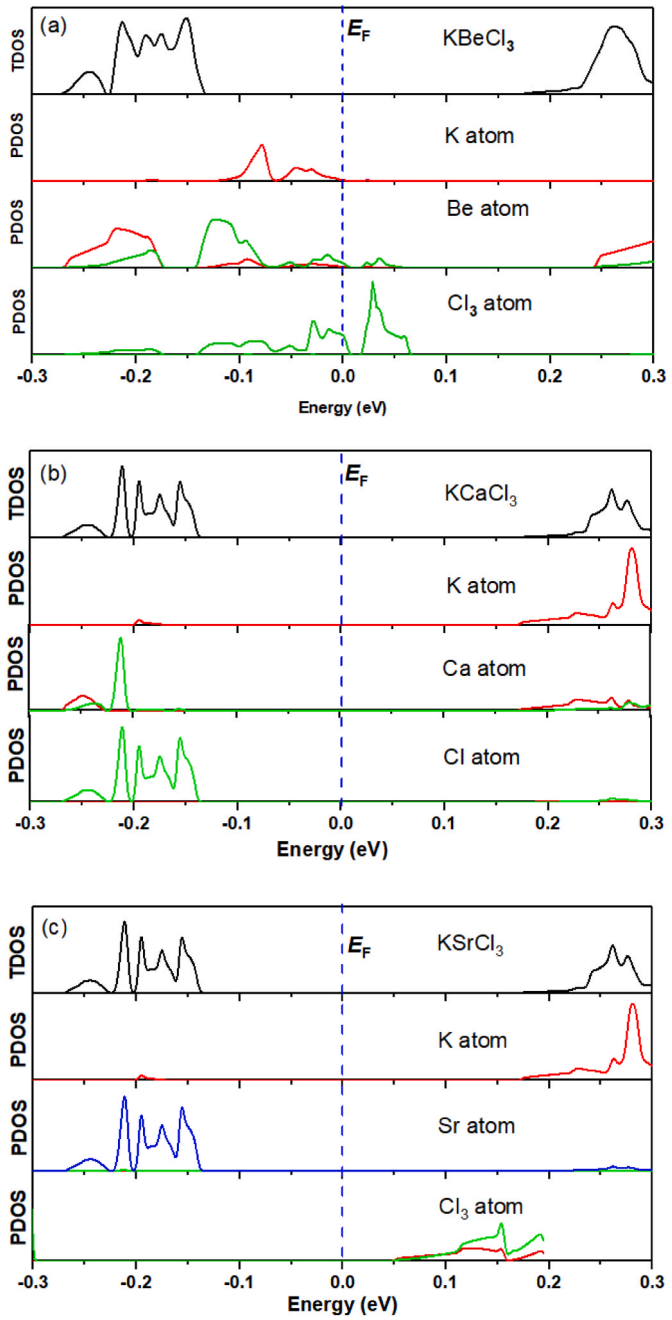

Fig. 4. TDOS and PDOS of (a) $KBeCl_3$ (b) $KCaCl_3$ (c) $KSrCl_3$ by using TB-mBJ functional. Red, green and blue lines refer to *s*-, *p*- and *d*-states, respectively. (For interpretation of the references to colour in this figure legend, the reader is referred to the Web version of this article.)

Voigt and Reuss bulk modulus for cubic crystal are given as follows [39]:

$$B_v = B_R = (C_{11} + 2C_{12})/3 \quad (3)$$

Similarly, Voigt and Reuss shear modulus for cubic crystal is [39]:

$$G_v = (C_{11} - C_{12} + 3C_{44})/5 \quad (4)$$

$$G_R = 5(C_{11} - C_{12})C_{44}/[4C_{44} + 3(C_{11} - C_{12})] \quad (5)$$

According to Hill approximation, the averages of Reuss and Voigt approximations are the efficient shear and bulk moduli which are represented as follows:

$$G = \tfrac{1}{2}(G_V + G_R),\ B = \tfrac{1}{2}(B_V + B_R)$$

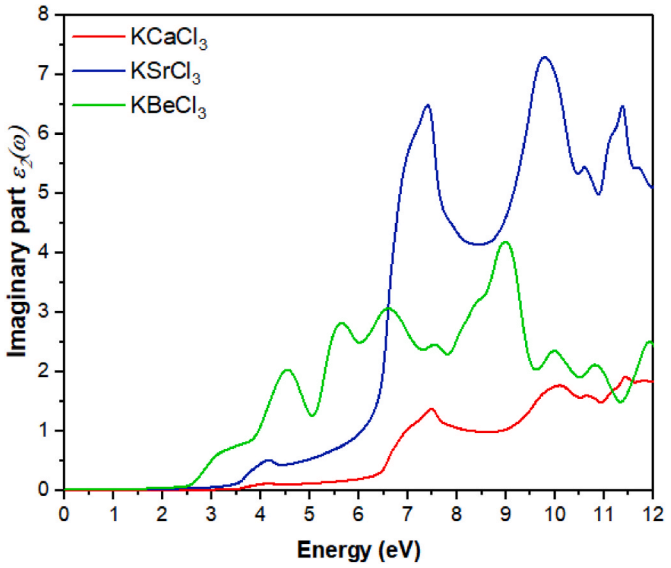

Fig. 5. Imaginary part $\epsilon_2(\omega)$ of the dielectric function for $KXCl_3$ (Be, Ca, and Sr).

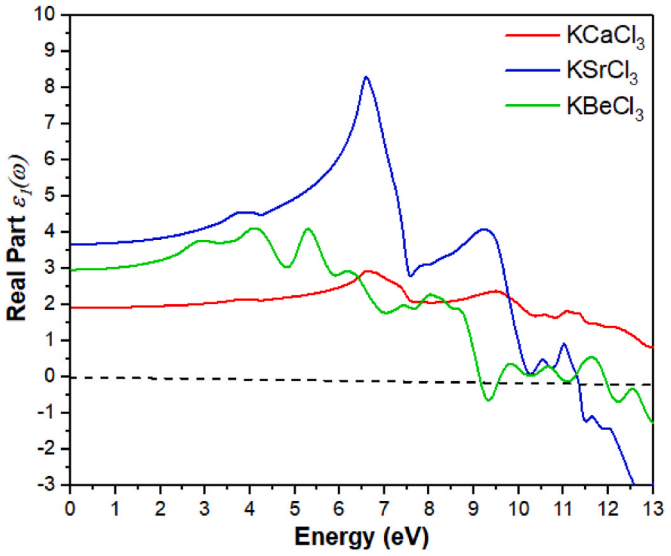

Fig. 6. Real part $\epsilon_1(\omega)$ of the dielectric function for $KXCl_3$ (Be, Ca, and Sr).

Bulk and shear modulus is the measurement of material resistance to change in volume and change in shape respectively. Young's modulus is the ratio of tensile stress to tensile strain and is used to measure the stiffness of the solid through this formula $E = \frac{9BG}{3B+G}$ [39] and are given in Table 4.

Moreover, mechanical properties include Poisson's ratio which discussed the bonding characteristics of compounds. However, if the values are around 0.1 then covalent characters and for the values around 0.25 ionic character is dominant in bonding. Poisson's ratio can be measured through this formula $\upsilon = 3B - 2G/2(3B + G)$ [40]. Pugh's modulus (G/B ratio) is also about bonding character. Although, for the ratio value 0.6 ionic character and 1.1 covalent character is dominant. Materials ductility and brittleness has been judged through B/G ratio. Materials having B/G ratio greater than 1.75 and less than 1.75 have ductile and brittle nature respectively. Vicker's hardness test is used to measure the hardness of the material and it can be obtained by using this formula:

$$H_V = 2(G^3/B^2)^{0.585} - 3 \quad (6)$$

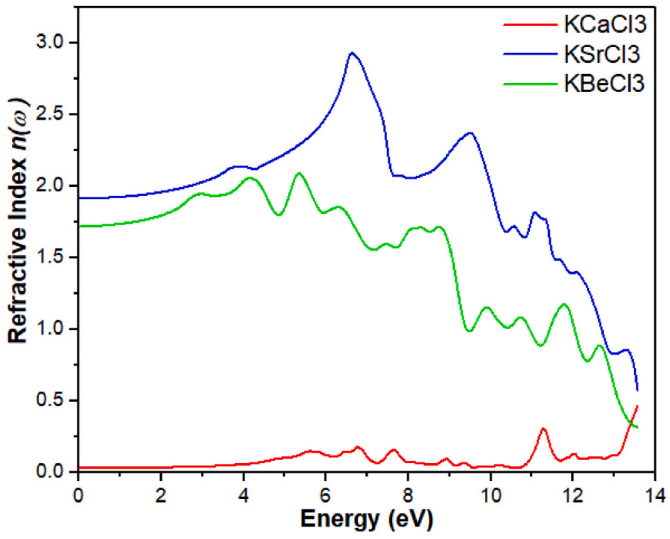

Fig. 7. Refractive index $n(\omega)$ for $KXCl_3$ (Be, Ca, and Sr).

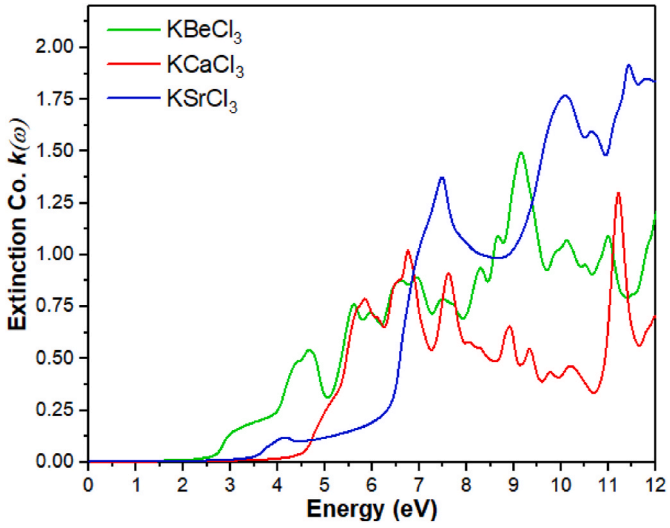

Fig. 8. Extinction coefficient $k(\omega)$ for $KXCl_3$ (Be, Ca, and Sr).

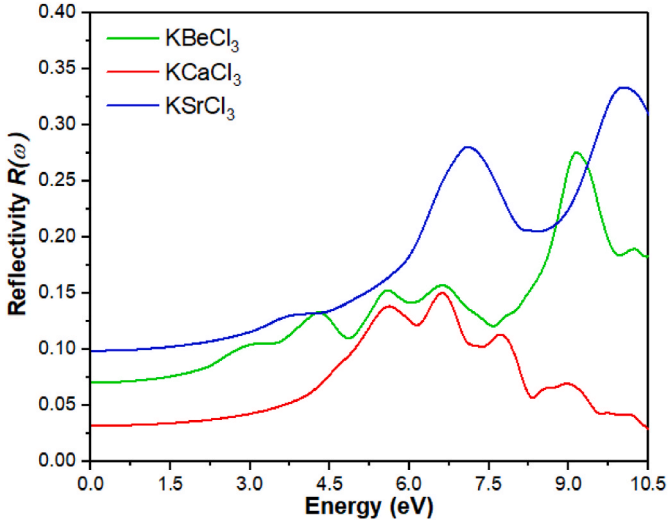

Fig. 9. Reflectivity $R(\omega)$ for $KXCl_3$ (Be, Ca, and Sr).

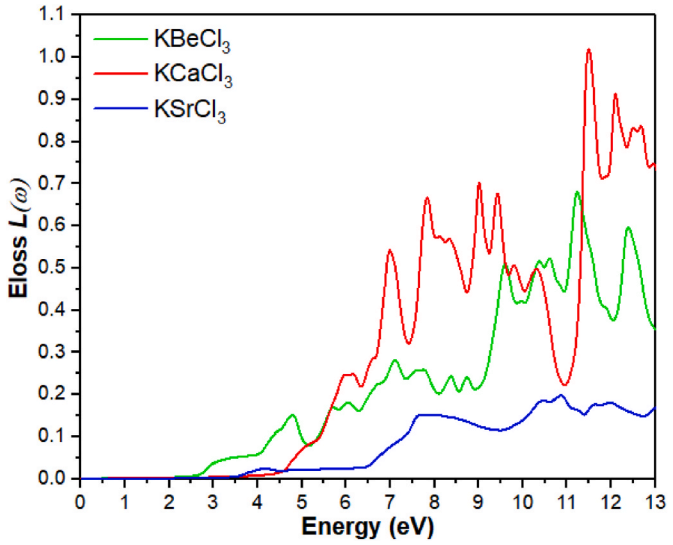

Fig. 10. Energy loss function L(ω) for $KXCl_3$ (Be, Ca, and Sr).

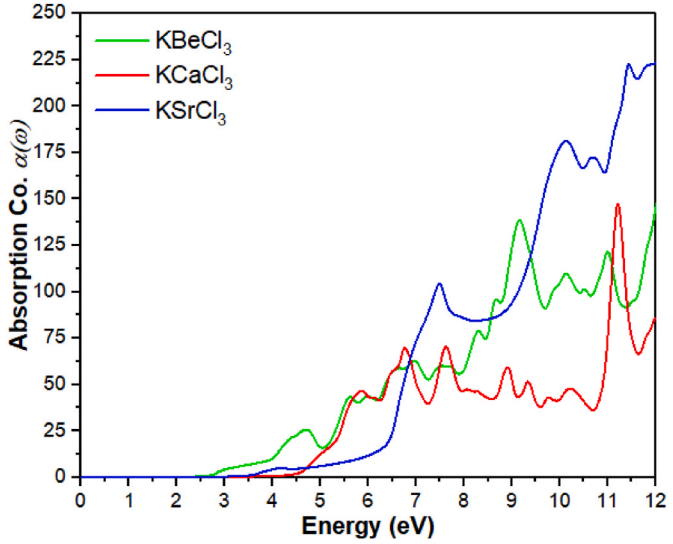

Fig. 11. Absorption coefficient $\alpha(\omega)$ for $KXCl_3$ (Be, Ca, and Sr).

Table 3
It represents three elastic constants.

Compounds	C_{11} (GPa)	C_{44} (GPa)	C_{12} (GPa)
$KBeCl_3$	568.83	18.74	44.99
$KCaCl_3$	1.85	7.57	1.39
$KSrCl_3$	343.05	−3987.80	312.18

Moreover, according to this hardness test if the theoretical values of materials are less than the hardness limit which is 40 GPa then these materials are relatively hard [40]. Table 5 represents values of different mechanical properties. According to the results of the Poisson ratio and pugh's modulus $KBeCl_3$ and $KSrCl_3$ both dominate ionic character in their bonding. Although in $KSrCl_3$ covalent character is dominant, both parameters verified each other results. However, values of B/G ratio show that materials $KBeCl_3$ and $KSrCl_3$ are ductile in nature and $KCaCl_3$ possess brittle nature. All three compounds are good hard materials proved by Vicker's hardness test values which are less than 40 GPa.

Table 4
It represents the Voigt, Reuss and Hill approximation values of bulk and shear moduli.

Compounds	B (GPa)	G (GPa)	E (GPa)	B_v	G_v	B_R	G_R
$KBeCl_3$	219.78	72.94	197.04	219.79	116.05	219.77	29.84
$KCaCl_3$	1.68	2.76	5.36	1.76	4.69	1.59	0.84
$KSrCl_3$	163.3	87.28	2.89	323.46	172.76	3.27	1.81

Table 5
Different elastic parameters.

Compounds	B/G	G/B	H_v (GPa)	υ
$KBeCl_3$	3.01	0.33	3.76	0.35
$KCaCl_3$	0.60	1.64	3.47	0.03
$KSrCl_3$	1.87	0.53	10.12	0.27

4. Conclusions

This theoretical investigation shows the structural, optoelectronic, and mechanical response of potassium-based perovskite $KXCl_3$ (X = Be, Ca and Sr) by employing the (LO + FP - LAPW) scheme within PBE-GGA exchange-correlation approximation. The volume optimization graph shows that these studied compounds are stable at minimum ground state energy. The computed band structure of the compounds depicted the indirect band-gap; and the band-gap values for $KBeCl_3$, $KCaCl_3$ and $KSrCl_3$ are 1.90, 3.85 and 4.20 eV respectively; the computed results presented that these semiconductors have wide band gap. Conversely; the optical properties are directly related to electronic band gap structure. It observed that at minimum energies 0–4.5 eV the approximately zero frequency change of the reflectivity spectra *R*(*0*) are 4%, 3%, and 9.8%, respectively. Relatively low reflectivity indicates extremely crystal clear materials through IR, visible, and the low frequency end of the UV range. Reflectivity and absorption related results making them key materials for absorption devices (opaqueness), and optoelectronic applications. Moreover, mechanically $KCaCl_3$ is found to be brittle while $KBeCl_3$ and $KSrCl_3$ as ductile material in their nature.

Declaration of competing interest

The authors declare that they have no known competing financial interests or personal relationships that could have appeared to influence the work reported in this paper.

References

[1] H.R. Wenk, A. Bulakh, Minerals: their constitution and origin, Can. Min. J. 125 (4) (2004) 7.
[2] W.S. Yang, J.H. Noh, N.J. Jeon, Y.C. Kim, S. Ryu, J. Seo, S.I. Seok, High-performance photovoltaic perovskite layers fabricated through intramolecular exchange, Science 348 (6240) (2015) 1234–1237.
[3] H. Zhou, Q. Chen, G. Li, S. Luo, T.B. Song, H.S. Duan, Y. Yang, Interface engineering of highly efficient perovskite solar cells, Science 345 (6196) (2014) 542–546.
[4] Z.K. Tan, R.S. Moghaddam, M.L. Lai, P. Docampo, R. Higler, F. Deschler, R. H. Friend, Bright light-emitting diodes based on organometal halide perovskite, Nat. Nanotechnol. 9 (9) (2014) 687–692.
[5] M.A. Haq, Md Saiduzzaman, T.I. Asif, I.K. Shuvo, K.M. Hossain, Ultra-violet to visible band gap engineering of cubic halide $KCaCl_3$ perovskite under pressure for optoelectronic applications: insights from DFT, RSC Adv. 11 (58) (2021) 36367–36378.
[6] I.K. Shuvo, Md Saiduzzaman, T.I. Asif, M.A. Haq, K.M. Hossain, Band gap shifting of halide perovskite $CsCaBr_3$ from ultra-violet to visible region under pressure for photovoltaic applications, Mater. Sci. Eng., B 278 (2022) 1–10.
[7] X. Liu, J. Fu, M.M. Han, K.X. Sun, S.L. Wei, First-Principles study on electronic structure, elasticity, debye temperature and anisotropy of cubic $KCaF_3$, Mater. Sci. Forum 999 (2020) 109–116.
[8] A.A. Mousa, First-principles study of structural, electronic and optical properties of the $KCaX_3$ (X= F and Cl) compounds, Int. J. Mod. Phys. B 28 (21) (2014) 1–15.
[9] S. Hayat, R.A. Khalil, M.I. Hussain, A.M. Rana, F. Hussain, A DFT study of perovskite type halides $KBeBr_3$, $RbBeBr_3$, and $CsBeBr_3$ in triclinic phase for advanced optoelectronic devices, Solid State Commun. 344 (2022) 1–16.
[10] S.K. Mitro, Md Saiduzzaman, A. Biswas, A. Sultana, K.M. Hossain, Electronic phase transition and enhanced optoelectronic performance of lead-free halide perovskites $AGeI_3$ (A= Rb, K) under pressure, Mater. Today Commun. 31 (2022) 1–9.
[11] K. Yang, Y. He, Y. Cheng, L. Che, L. Yao, First-principles calculations on the structural and electronic properties of cubic $KCaF_3$ and $NaCaF_3$ (001) surfaces, Phys. Lett. 381 (9) (2017) 890–895.
[12] Y.I. Dolzhenko, T. Inabe, Y. Maruyama, In situ X-ray observation on the intercalation of weak interaction molecules into perovskite-type layered crystals ($C_9H_{19}NH_3$) $2PbI_4$ and ($C_{10}H_{21}NH_3$) $2CdCl_4$, Bull. Chem. Soc. Jpn. 59 (2) (1986) 563–567.
[13] A. Kojima, K. Teshima, Y. Shirai, T. Miyasaka, Organometal halide perovskites as visible-light sensitizers for photovoltaic cells, J. Am. Chem. Soc. 131 (17) (2009) 6050–6051.
[14] Q. Mahmood, U.H. Bakhtiar, M. Yaseen, M.R. Shahid, M.G.B. Ashiq, A. Mahmood, The first-principle study of mechanical, optical and thermoelectric properties of $SnZrO_3$ and $SnHfO_3$ for renewable energy applications, Solid State Commun. 292 (2019) 17–23.
[15] A. Lamichhane, N.M. Ravindra, Isosymmetric compression of cubic halide perovskites ABX_3 (A= K, Rb, Cs; B= Ge, Sn, Pb and X= Cl, Br, I)-influence of cation–anion exchange: a first principle study, SN Appl. Sci. 3 (2021) 1–12.
[16] P. Pitriana, T.D.K. Wungu, R. Hidayat, The characteristics of band structures and crystal binding in all-inorganic perovskite $APbBr_3$ studied by the first principle calculations using the Density Functional Theory (DFT) method, Results Phys. 15 (2019) 1–20.
[17] B. Sabir, G. Murtaza, R.A. Khalil, Q. Mahmood, First principle study of electronic, mechanical, optical and thermoelectric properties of $CsMO_3$ (M= Ta, Nb) compounds for optoelectronic devices, J. Mol. Graph. 86 (2019) 19–26.
[18] K. Khan, J. Sahariya, A. Soni, Structural, electronic and optical modeling of perovskite solar materials $ASnX_3$ (A= Rb, K; X= Cl, Br): first principle investigations, Mater. Chem. Phys. 262 (2021) 1–9.
[19] P. Blaha, K. Schwarz, G.K. Madsen, D. Kvasnicka, J. Luitz, An Augmented Plane Wave + Local Orbitals Program for Calculating Crystal Properties, Karlheinz Schwarz, Techn, Universiïat Wien, Austria, 2001.
[20] Y. Zhang, W. Yang, Comment on "Generalized gradient approximation made simple", Phys. Rev. Lett. 80 (4) (1998) 890.
[21] F. Tran, P. Blaha, Accurate band gaps of semiconductors and insulators with a semilocal exchange-correlation potential, Phys. Rev. Lett. 102 (22) (2009) 1–4.
[22] N. Ahmed, J. Nisar, R. Kouser, A.G. Nabi, S. Mukhtar, Y. Saeed, M.H. Nasim, Study of electronic, magnetic and optical properties of KMS_2 (M= Nd, Ho, Er and Lu): first principle calculations, Mater. Res. Express 4 (6) (2017) 1–11.
[23] S. Haid, W. Benstaali, A. Abbad, B. Bouadjemi, S. Bentata, Z. Aziz, Thermoelectric, structural, optoelectronic and magnetic properties of double perovskite Sr_2CrTaO_6: first principle study, Mater. Sci. Eng. B 245 (2019) 68–74.
[24] F. Mouhat, F.X. Coudert, Necessary and sufficient elastic stability conditions in various crystal systems, Phys. Rev. B 90 (22) (2014) 1–4.
[25] A. Ali, A.U. Rahman, G. Rahman, Thermoelectric properties of $KCaF_3$, Phys. B Condens. Matter 565 (2019) 18–24.
[26] L. Li, Y.J. Wang, D.X. Liu, C.G. Ma, M.G. Brik, A. Suchocki, A.H. Reshak, Comparative first-principles calculations of the electronic, optical, elastic and thermodynamic properties of $XCaF_3$ (X= K, Rb, Cs) cubic perovskites, Mater. Chem. Phys. 188 (2017) 39–48.
[27] B. Erdinc, Density functional calculations of the electronic band structure and optical properties of KCaF3, GU J. Sci. 24 (4) (2011) 671–677.
[28] B. Ghebouli, M. Fatmi, M.A. Ghebouli, H. Choutri, L. Louail, T. Chihi, A. Bouhemadou, S. Bin-Omran, Theoretical study of the structural, elastic, electronic and optical properties of $XCaF_3$ (X= K and Rb), Solid State Sci. 43 (2015) 9–14.
[29] Z. Xiao, Y. Yan, Progress in theoretical study of metal halide perovskite solar cell materials, Adv. Energy Mater. 7 (22) (2017) 1–20.
[30] D.Y. Heo, S.M. Han, N.S. Woo, Y.J. Kim, T.Y. Kim, Z. Luo, S.Y. Kim, Role of additives on the performance of $CsPbI_3$ solar cells, J. Phys. Chem. C 122 (28) (2018) 15903–15910.
[31] G. Murtaza, I. Ahmad, First principle study of the structural and optoelectronic properties of cubic perovskites $CsPbM_3$ (M= Cl, Br, I), Phys. B Condens. Matter 406 (17) (2011) 3222–3229.
[32] R. Abt, C. Ambrosch-Draxl, P. Knoll, Optical response of high temperature superconductors by full potential LAPW band structure calculations, Phys. B Condens. Matter 194 (1994) 1451–1452.
[33] C. Ambrosch-Draxl, J.A. Majewski, P. Vogl, G. Leising, First-principles studies of the structural and optical properties of crystalline poly (para-phenylene), Phys. Rev. B 51 (15) (1995) 9668–9676.
[34] C. Ambrosch-Draxl, J.O. Sofo, Linear optical properties of solids within the full-potential linearized augmented planewave method, Comput. Phys. Commun. 175 (1) (2006) 1–14.
[35] D. Pan, Q. Wan, G. Galli, The refractive index and electronic gap of water and ice increase with increasing pressure, Nat. Commun. 5 (1) (2014) 1–6.

[36] G. Tse, D. Yu, The first principle study: electronic and optical properties in Bi_2Se_3, Comput. Condens. Matter 4 (2015) 59–63.
[37] Z.J. Wu, E.J. Zhao, H.P. Xiang, X.F. Hao, X.J. Liu, J. Meng, Crystal structures and elastic properties of superhard IrN_2 and IrN_3 from first principles, Phys. Rev. B 76 (5) (2007) 1–15.
[38] Y. Wen, L. Wang, H. Liu, L. Song, Ab initio study of the elastic and mechanical properties of B19 TiAl, Crystals 7 (2) (2017) 39.
[39] D. Connétable, O. Thomas, First-principles study of the structural, electronic, vibrational, and elastic properties of orthorhombic NiSi, Phys. Rev. B 79 (9) (2009) 1–10.
[40] G. Surucu, A. Gencer, A. Candan, H.H. Gullu, M. Isik, $CaXH_3$ (X= Mn, Fe, Co) perovskite-type hydrides for hydrogen storage applications, Int. J. Energy Res. 44 (3) (2020) 2345–2354.